Icarus 455 (2026) 117107

Contents lists available at ScienceDirect

Icarus

journal homepage: www.elsevier.com/locate/icarus

Comparative analysis of meteor spectra observed simultaneously from multiple locations☆

Veronika Pazderová [a],*, Pavol Matlovič [a], Hadrien A.R. Devillepoix [b,c]

[a] Faculty of Mathematics, Physics and Informatics, Comenius University, Mlynská Dolina, Bratislava, 842 48, Slovakia
[b] Space Science and Technology Centre, School of Earth and Planetary Sciences, Curtin University, Kent Street, Perth, 6102, WA, Australia
[c] International Centre for Radio Astronomy Research, Curtin University, Perth, 6845, WA, Australia

ARTICLE INFO

Keywords:
Meteors
Meteoroids
Spectroscopy
Observational techniques

ABSTRACT

Meteor spectroscopy is a key method for probing the composition of meteoroids, providing insights into both their overall composition and the relative abundances of individual species. In this study, we present a comparison of meteor spectra recorded simultaneously from multiple observing sites within the Australian segment of the AMOS (All-sky Meteor Orbit System) network. We examine the origins of spectral discrepancies between the respective systems, considering factors such as focusing, spectrum extraction geometry, calibration, and observing geometry. This work represents one of the few detailed examinations of such effects. Our results show that factors like observing geometry, focusing, calibration procedures, instrument characteristics, and specific data-processing approaches can introduce uncertainties in relative line intensities that are typically unresolved in conventional single-station observations. The four case studies presented in this work demonstrate that the sources of discrepancies in relative line intensities can be identified and potentially accounted for, ensuring that meteoroid composition estimates based on these intensities remain robust.

1. Introduction

Meteor spectroscopy represents the most direct and accessible method for constraining the composition of meteoroids. When combined with complementary approaches, such as meteorite fall studies (as recently demonstrated in the case of the Ribbeck meteorite by Spurný et al. (2024)) and laboratory experiments simulating meteoroid ablation (comprehensively described by Tóth et al. (2024) and Matlovič et al. (2024)), spectral observations provide unique insights into both the elemental makeup and the overall compositional classification of meteoroids. These insights can be obtained either through detailed modelling of meteor spectra to derive quantitative relative elemental abundances (e.g., Borovička 1993, Trigo-Rodríguez et al. 2003, Jenniskens 2007, Ferus et al. 2018, Drouard et al. 2018) or by assigning meteoroids to material groups recognised in meteorite taxonomy based on the specific relative intensity ratios of specific emission features (Borovička et al., 2005 or Matlovič et al., 2026). The modelling of meteor radiation is typically performed by fitting observed spectra with synthetic profiles generated using radiative transfer models that assume local thermal equilibrium and account for self-absorption in the radiating plasma (Borovička, 1993). Approaches based on direct comparison of multiplet intensities, such as the scheme of Borovička et al. (2005), which employs the relative intensities of Mg I-2, Fe I-15, and Na I-1 to evaluate meteoroids' correspondence with a chondritic composition, likewise depend directly on the observed intensities of spectral lines. Because these approaches are inherently direct and involve certain simplifications and limitations, several important factors must be considered in their application.

One such factor is that the composition of the radiating plasma envelope surrounding a meteoroid during its atmospheric flight does not exactly correspond to the elemental composition of the meteoroid itself. This discrepancy is particularly evident for refractory elements such as aluminium, calcium, and titanium, whose underrepresentation in the plasma is most likely a consequence of their incomplete evaporation (Borovička 1993, Trigo-Rodríguez et al. 2003, Kasuga et al. 2005, Matlovič et al. 2024). Additional influences on the resulting spectra arise from the observational conditions, the characteristics of the instruments employed, the calibration procedures applied during data reduction, and the overall quality of the observations.

Instrumental factors and calibration have been examined in detail by Šegon and Borovička (2023) and, most comprehensively, by Šegon et al. (2024). Both studies described cases of meteors, whose spectra were recorded from multiple observing sites, revealing differences

☆ This article is part of a Special issue entitled: 'Meteoroids 2025' published in Icarus.

* Corresponding author.
E-mail address: veronika.pazderova@fmph.uniba.sk (V. Pazderová).

https://doi.org/10.1016/j.icarus.2026.117107
Received 14 January 2026; Received in revised form 10 March 2026; Accepted 14 April 2026
Available online 17 April 2026

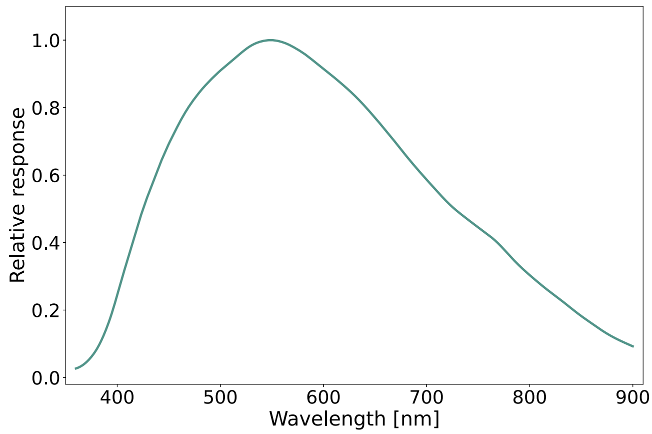

Fig. 1. Spectral response curve of the AMOS-Spec-HR spectrographs.

in relative line intensities despite the expectation that proper calibration should yield nearly identical results. In Šegon et al. (2024), the authors identified the causes of these discrepancies, showing that relative line intensities depend both on the position of the spectral features within the field of view (FOV) and on their wavelength. These dependencies arise from the combined effects of wide-angle optics, dispersive elements, detector response, and atmospheric transmission. Consequently, identical spectral features observed at different positions in the FOV may exhibit varying intensities due to vignetting, distortion, and angle-dependent throughput. Furthermore, the overall sensitivity of the optical system and detector is strongly wavelength-dependent, with shorter wavelengths attenuated more severely by both the instrument's response curve and atmospheric extinction. The magnitude of these effects depends on the specific observational setup used during spectra acquisition.

The influence of observing geometry on meteor spectroscopy was examined in detail by Kubelík et al. (2022). Through complex plasma radiation modelling, the study demonstrated that both the viewing geometry and the non-homogeneous structure of the radiating plasma surrounding ablating meteoroids affect the recorded spectra, as illustrated by the case of a bright Leonid bolide. Spatial inhomogeneities in plasma temperature and electron density had already been suggested by Borovička (1993), implying that different lines of sight intersecting distinct regions of the plasma can produce spectra that vary with the relative position of the meteor and the observer. As shown by Kubelík et al. (2022), as the angle between the meteor's velocity vector and the observer's line of sight decreases, the line of sight progressively traverses hotter plasma near the meteor shock wave, thereby enhancing the contribution of the high-temperature spectral component (Borovička, 1994). This effect is expected to be most pronounced in meteors observed in a head-on orientation relative to the observing instrument.

Although the topic is not entirely unexplored, relatively few studies have examined in detail the differences between meteor spectra recorded simultaneously from multiple observing sites. The AMOS network, designed and operated by researchers at Comenius University in Bratislava, currently comprises 17 all-sky systems and 19 spectrographs deployed worldwide (Tóth et al., 2026), enabling relatively frequent observations of meteors with spectra captured simultaneously from several locations. The AMOS spectral database now contains approximately 200 such observations, spanning a wide range of properties including observing geometry, FOV position, spectral resolution, and brightness. This dataset therefore provides an excellent opportunity for qualitative studies of spectral variability under different observing conditions. In this paper, we illustrate these differences and the complexity of the problem through four meteors, chosen to form a small but diverse set of case studies with distinct characteristics.

Section 2 provides a brief description of the AMOS instrumentation and the spectral processing pipeline used for meteor spectra reduction. Section 3 presents the four case studies in detail. Finally, Section 4 summarises the findings from these case studies, reviews all plausible sources of discrepancies observed in multi-station spectra, outlines possible mitigation measures, and assesses their impact on meteoroid composition estimates based on relative line-intensity ratios for the AMOS-Spec-HR instrument.

2. Instrumentation and data processing

All meteor spectra presented in the following sections were acquired using spectrographs of the AMOS network. The analysed spectra come from the high-resolution AMOS-Spec-HR slitless spectrographs, each equipped with a 6 mm f/1.4 lens coupled to a DMK 33UX252 digital camera operating at 20 fps. This setup provides a pixel resolution of 2048×1536 ($1.76\,\mathrm{arcmin\ px^{-1}}$), FOV of $60° \times 45°$, and is supplemented with a $1000\,\mathrm{gr\,mm^{-1}}$ holographic grating with a dispersion of $0.5\,\mathrm{nm\,px^{-1}}$, which corresponds to a resolving power of R $\approx$ 550. The AMOS-Spec-HR enables observation of higher-resolution meteor spectra with typical full width at half maximum (FWHM) values around 1.2 nm in the visible range. The limiting stellar magnitude of the setup is approximately +4, while the limiting magnitude required for the detection of first-order meteor spectra is approximately -1.5.

The spectral reduction process is carried out on flat-field corrected video recordings with background subtraction to reduce noise levels and suppress additional illumination sources. Time-integrated spectra are obtained by manually scanning all individual video frames containing the spectrum, converting the scale from pixel coordinates to wavelengths, summing the signal across all relevant frames, and calibrating the resulting profiles for camera sensitivity and atmospheric extinction. Calibration is performed by dividing each spectral profile first by an appropriate instrumental response curve (Fig. 1) and subsequently by an atmospheric transmittance function provided by the TAPAS[1] online service (Bertaux et al., 2014; Lallement et al., 2025). The resulting spectra are fitted with synthetic spectral profiles using the damped least-squares method (Levenberg–Marquardt algorithm) implemented in the FITYK software (Wojdyr, 2010). Line intensities are derived by integrating the profiles of selected spectral lines, with multiplet numbers assigned according to Moore (1945).

The atmospheric trajectories of the majority of the discussed meteors were determined from data obtained by AMOS-Cam all-sky cameras. Each AMOS-Cam system comprises a fisheye lens, an image intensifier, a projection lens, and a digital video camera with a pixel resolution of 1600×1200, a FOV of $180° \times 140°$ ($6.8\,\mathrm{arcmin\,px^{-1}}$), and a frame rate of 20 fps. The limiting stellar magnitude of AMOS-Cam is approximately +5 mag for single-frame detections and about +4 mag for moving objects, as a result of trailing losses. The specific trajectories were estimated using an updated version of the MT (Meteor Trajectory) software, developed for the processing of AMOS data and previously described in Kornoš et al. (2018). Further details on the AMOS instrumentation and reduction procedures are provided in Tóth et al. (2026). An example of a typical AMOS system and the AMOS-Spec-HR spectrum can be found in Fig. 2.

3. Study cases

The study cases presented in the following sections originate from the subset of AMOS network deployed on Australia's Nullarbor Plain, which presently hosts three all-sky AMOS-Cam systems and eight spectrographs: one at Kybo (KY), one at Mundrabilla (MU), and six at Forrest (FO), as illustrated in Fig. 3. All AMOS spectral observations in Australia are carried out in collaboration with the Desert Fireball

[1] TAPAS online service

Fig. 2. Upper panel: typical configuration of the AMOS system, comprising the all-sky AMOS-Cam and the AMOS-Spec-HR spectrograph (shown in the lower left corner). Lower panel: composite image of meteor M20240725_140350 recorded by the AMOS-Spec-HR located on Mauna Kea, Hawaii.

Network (DFN) (Devillepoix et al., 2022). In addition to multi-station detections across all three Australian sites, the number of AMOS-Spec-HR spectrographs at Forrest provides near full-sky coverage, making simultaneous recordings of individual meteors by multiple spectrographs at Forrest fairly common. The four meteor case studies presented in this paper were specially selected to exemplify diverse observing geometries, variable spectral resolution, brightness and saturation levels that typically affect the observations of meteor spectra. In all analysed study cases, the relative line intensities are derived from time-integrated spectra constructed from frames sharing identical timestamps across all observing stations, ensuring that all spectra correspond to the same altitude interval along the meteor trajectory. This approach explicitly avoids mixing spectral data originating from different ablation regimes or dynamical phases of the flight, which would introduce inconsistencies in the integrated energy and compromise the physical comparability of the measurements across multiple cameras.

3.1. M20231017_172212

M20231017_172212 was a sporadic meteor of absolute magnitude −6.9 mag originating from a Jupiter-family comet (JFC) trajectory, with initial speed of $v_i = 24.2\,\mathrm{km\,s^{-1}}$. It was recorded by three AMOS all-sky systems and four spectral instruments: Spec-MU, Spec-KY, Spec-FONW, and Spec-FOSW, yielding four spectra from three distinct observing sites, presented in Fig. 4. The dominant spectral features observed across all profiles correspond to emission of Fe I, Mg I, Na I, Cr I, and Mn I (Fig. 5). Their presence and relative intensities are consistent with emission spectra of typical asteroidal meteoroids of chondritic composition. This interpretation is further supported by the detection and relative intensities of Ti I and Ni I lines in all spectra (Matlovič et al., 2024). Notably, all available M20231017_172212 spectra show no detectable calcium lines.

Although broadly similar, the M20231017_172212 spectra displayed in Figs. 4 and 5 reveal notable differences in quality and characteristics. The faintest yet relatively sharp spectrum recorded by Spec-MU exhibits a weak near-UV region, with spectral lines having FWHM values ranging from approximately 1.1 nm in the green to 1.6 nm in the near-UV. Instrumentally, AMOS-Spec-HR systems achieve higher resolution in the near-UV than in the visible/red, and this opposite trend is most likely a consequence of imperfect focusing. The FOV position of Spec-MU spectrum is close to that of Spec-FOSW, whose spectrum, while displaying a clearly defined near-UV region, is the lowest quality of the four, with some lines broadened to as much as 3.5 nm FWHM. The spectrum captured by Spec-FONW was recorded under a large inclination angle relative to the horizontal dispersion direction, which complicated the scanning process and produced considerable line broadening, up to 2.0 nm FWHM across the entire wavelength range. The Spec-KY spectrum has a resolution comparable to Spec-MU, but differs in other important aspects. Unlike the other three spectral observations of M20231017_172212, it exhibits significant saturation throughout the spectral profile. Additionally, its initial phases occurred outside the spectrograph's FOV, so the earliest stage of ablation is missing. The time-integrated spectra of M20231017_172212 in Fig. 5 were therefore obtained by combining 15 representative profiles taken from recording frames with the lowest saturation. These frames were selected primarily from the middle portion of the meteor trajectory to avoid the early and late stages of ablation, where differential ablation (Borovička, 1993; von Zahn et al., 1999; Abe, 2009; Matlovič et al., 2020) and the early release of volatiles may significantly influence the resulting relative line intensities.

The most significant factors influencing the line profiles and intensities of M20231017_172212 spectra are most likely related to focusing, spectrum extraction geometry, and calibration. The overall quality and spectral resolution of the individual profiles are illustrated in Fig. 5, where the resolving power ranges from $R \approx 400$ for Spec-FONW to $R \approx 800$–900 for the Spec-MU and Spec-KY profiles. A decrease in resolving power is occasionally observed in AMOS spectra recorded near the edges of the FOV, where off-axis rays are subject to stronger aberrations and focus errors. These effects broaden spectral lines and reduce resolution relative to the optical axis. Such distortions may be further amplified under extreme weather conditions, when strong winds typical for this region induce slight vibrations of the spectrographs and distort the spectra.[2] Although for M20231017_172212 no clear correlation is evident between spectrum quality and FOV position (the Spec-KY spectrum, recorded at the very top of the FOV, exhibits significantly higher quality than the Spec-FONW and Spec-FOSW spectra recorded closer to the centre of the FOV), the windy conditions prevailing during the observations may have contributed to the reduced quality of the Spec-FONW and Spec-FOSW spectra. Furthermore, the Spec-FONW profile is affected by non-ideal extraction and diffraction geometry — the acute angle at which this spectrum was recorded produced a notable signal overlap and line broadening, despite the use of a narrow scanning aperture.

[2] This issue has been resolved by reinforcing the construction of the AMOS spectrographs deployed in Nullarbor.

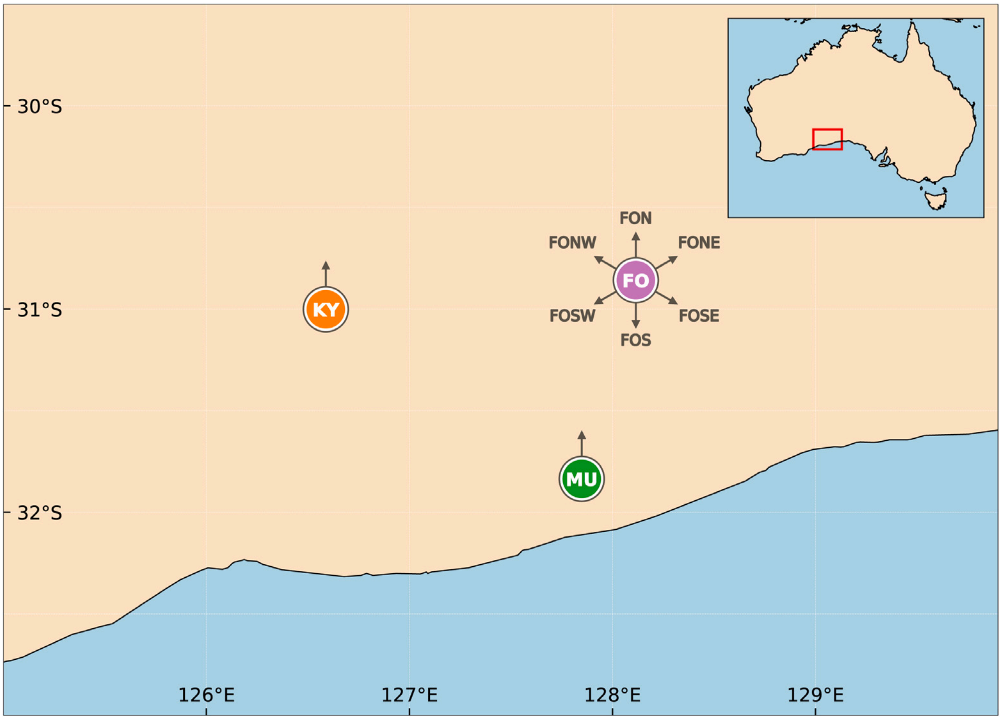

Fig. 3. Layout of the AMOS network in Australia, showing the stations MU (Mundrabilla), KY (Kybo), and FO (Forrest). Arrows radiating from each station indicate the pointing directions of the AMOS spectrographs installed at these sites.

Fig. 4. Composite image displaying the spectrum of M20231017_172212 recorded by four AMOS spectrographs: Spec-MU, Spec-KY, Spec-FONW, and Spec-FOSW. The layout of these instruments is shown in Fig. 3.

One of the strongest influences on the resulting spectra most likely arises from the calibration applied on the M20231017_172212 profiles. As described in Section 2, all AMOS spectra are calibrated for the spectral sensitivity of the instrument and for atmospheric extinction. The response curve for AMOS-Spec-HR, shown in Fig. 1, demonstrates that the largest correction is required in the near-UV, while the maximum sensitivity is reached in the green, at approximately 550 nm. Although grating efficiencies and detectors' quantum efficiencies may differ slightly or vary over time among the individual spectrographs, these effects are considered negligible in case of AMOS spectra. The most significant correction is introduced through atmospheric extinction, which predominantly affects the near-UV portion of the spectrum. Its magnitude depends strongly on the meteor's position: the closer the meteor is observed to the horizon, the weaker the atmospheric transmittance due to the increased optical path length. The overall impact of these calibrations is clearly visible in Fig. 5. While the region between 515 – 560 nm appears relatively consistent across the analysed profiles, with differences arising mainly from spectral resolution, the near-UV region exhibits more pronounced intensity discrepancies. While the TAPAS service provides robust model-based transmittance functions, its accuracy is somewhat limited by the absence of real-time local meteorological inputs, such as aerosol contents, humidity, and transient weather conditions. Additionally, differences in the zenith angle (altitude) of the meteor between the observing sites alter the effective optical path length through the atmosphere, which may lead to cumulative discrepancies in the resulting spectra, especially in the near-UV.

The comparison of the intensities of the Mn I-2 triplet (located at 403.08, 403.31, and 403.45 nm) across all four M20231017_172212 spectral profiles in Fig. 5 reveals a discrepancy that cannot be explained solely by measurement uncertainties or calibration errors. Although the varying resolution between the profiles inevitably distorts this part of the spectrum, in three out of four measured profiles (Spec-FONW, Spec-FOSW, Spec-MU) the Mn I-2 triplet is either weaker or comparable in intensity to the adjacent Fe I-43 line at 404.58 nm. In contrast, in the case of Spec-KY, Mn I-2 clearly peaks above the adjacent Fe I-43 line. This behaviour may indicate an influence of the observing geometry on the resulting spectral profiles, since the relative position between the M20231017_172212 meteor and Spec-KY slightly differed from that of the other instruments (Fig. 6). Differences in lines of sight between observing systems can introduce various physical effects that affect the recorded spectra, as demonstrated by the modelling of Kubelík et al. (2022). Depending on the viewing angle, lines of sight may traverse different regions of the radiating plasma, leading to variations in optical depth, self-absorption, and line-of-sight integration effects for specific species. Moreover, different viewing geometries may sample distinct portions of the shock front or ablation zone, which may alter the apparent line intensities. To further investigate this effect in the M20231017_172212 profiles, similar behaviour was examined in other

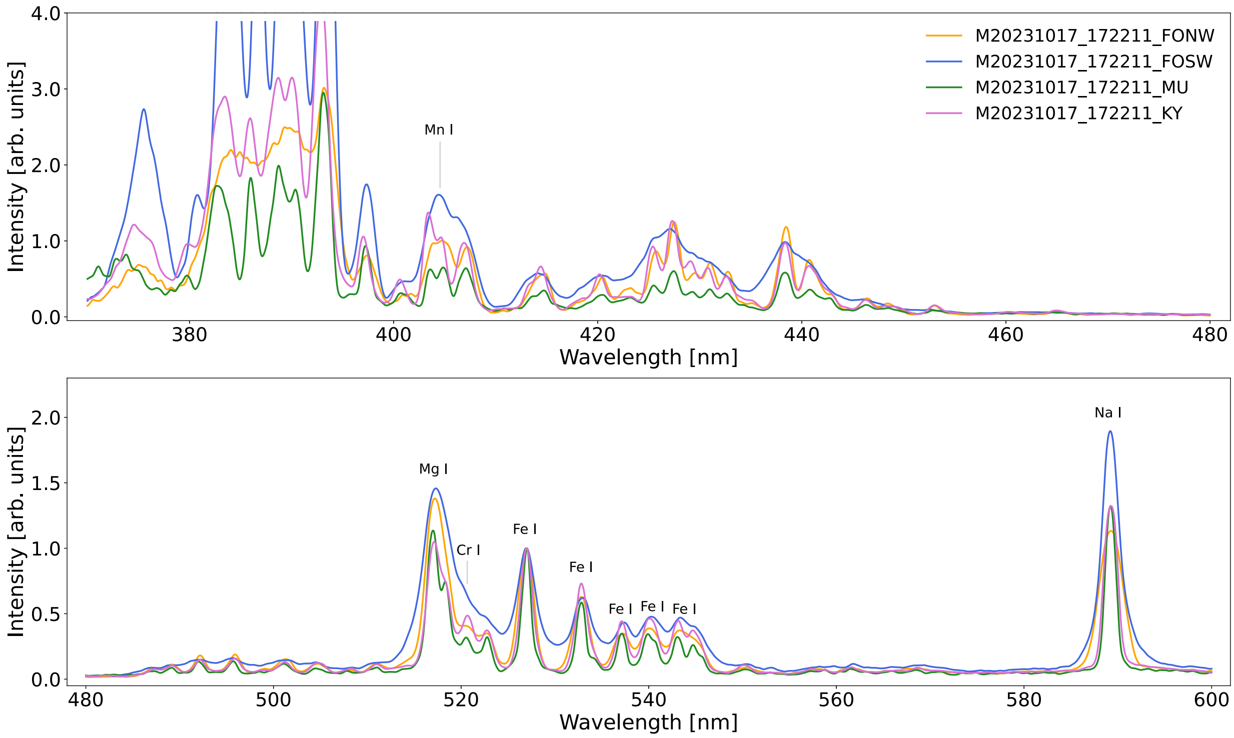

Fig. 5. Spectral profiles of meteor M20231017_172212 extracted from four AMOS-Spec-HR spectrographs: Spec-FONW, Spec-FOSW, Spec-MU, and Spec-KY. The layout of these instruments is shown in Fig. 3, and the suffixes attached to the meteor designation in the legend indicate the specific spectrograph from which each profile was obtained. For clarity, the spectra are divided into two wavelength ranges: 370–480 nm (upper panel) and 480–600 nm (lower panel). All profiles are normalised to unity at the peak of the Fe I-15 line at 526.95 nm, with several spectral lines of interest highlighted. The noticeable amplitude difference between the FONW and FOSW spectra in the 380–400 nm region arises most probably from residual uncertainties in the near-UV calibration, as discussed in Section 3.1.

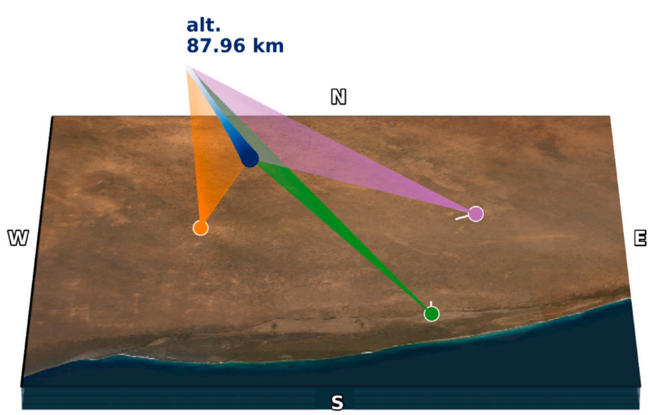

Fig. 6. Three-dimensional model of the M20231017_172212 atmospheric trajectory (blue gradient) relative to the AMOS systems at Kybo, Mundrabilla, and Forrest. The colour coding of these stations follows that used in Fig. 3. Short white lines radiating from the station positions indicate the orientations of the spectrographs that recorded the spectrum of M20231017_172212. The highlighted altitude corresponds to the meteor's beginning height. (For interpretation of the references to colour in this figure legend, the reader is referred to the web version of this article.)

low-excitation lines such as Fe I-1, Fe I-2, and Na I-1, but the results are inconclusive. The Na I-1 doublet (588.97 and 589.56 nm) is influenced by saturation (Spec-KY), line broadening due to spectrum extraction geometry (Spec-FONW), or focusing effects (Spec-FOSW). The Fe I-1 and Fe I-2 lines do exhibit some variations among the M20231017_172212 profiles, but they are either too weak or too blended with noise or other stronger lines to exclude the possibility that these differences arise from measurement uncertainties.

All of the aforementioned instrumental and calibration effects ultimately manifest as variations in the relative line intensities of meteor spectra. Since such relative intensities form the basis for deriving meteoroid composition, systematic differences introduced by atmospheric extinction correction, focusing, extraction and observing geometry, and other related factors may influence the accuracy of compositional analyses. The relative intensities of selected multiplets extracted from all M20231017_172212 spectral profiles are shown in Figs. 7–9 and are discussed further in Section 4.

3.2. M20231024_110038

Reconstruction of the atmospheric trajectory of meteor M20231024_110038 was impeded by adverse weather conditions at the time of the event. Nevertheless, data obtained by the DFN stations enabled a determination of its trajectory and an estimated entry velocity of $v_i = 16.9\,\mathrm{km\,s^{-1}}$. A geometric triangulation combined with a dynamical analysis based on the joint AMOS and DFN dataset indicates that M20231024_110038 may have produced a meteorite fall, with a surviving mass potentially reaching up to 50 g, although a terminal mass closer to 20 g is more probable. The emission spectrum of M20231024_110038 was recorded by the Spec-KY, Spec-FONW, and Spec-FOSW spectrographs (Fig. 10). The Spec-FOSW profile was excluded from further analysis due to its insufficient quality. Across the two high-quality spectra, the meteor exhibits features characteristic of asteroidal meteoroids of chondritic composition. The most prominent spectral features in the observed spectra belong to the Mg I-2, Fe I-15, and Na I-1 multiplets, all of which exhibit relatively strong saturation across the captured spectra. Additional notable features include other Fe I lines, as well as lines of Mn I, Cr I, and Ti I. (Fig. 10). The relative

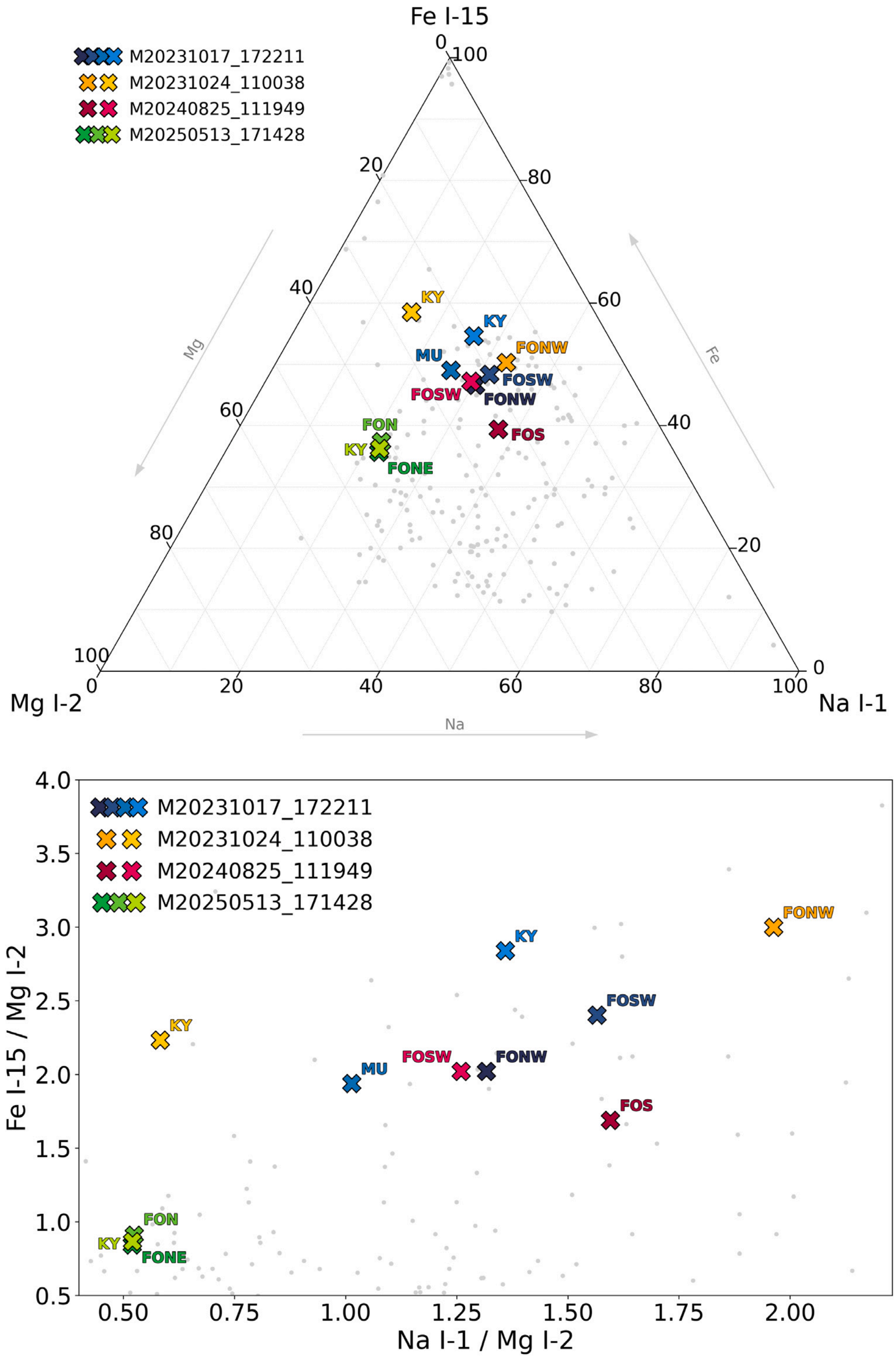

Fig. 7. Relative intensities of multiplets Mg I-2, Fe I-15, and Na I-1 extracted from the spectra of all meteors analysed in this work. Upper panel: ternary diagram illustrating the relative intensities of these multiplets for all spectral profiles discussed in Section 3. Grey points represent spectra of single-station meteors from the AMOS spectral database. Lower panel: correlation between the intensities of multiplets Fe I-15 and Na I-1 relative to Mg I-2 across all analysed spectra.

intensities of some of these multiplets are presented in Figs. 7 to 9 and examined in more detail in Section 4.

The atmospheric trajectory of M20231024_110038 clearly indicates that the meteor exhibited an almost head-on orientation relative to the Spec-KY spectrograph. As a result, the object appears as a luminous, quasi-spherical source rather than an elongated meteor trail in Fig. 10. Due to the pronounced saturation of the Spec-KY spectrum during nearly the entire observational interval, the spectral analysis was restricted to the initial phase of ablation. The final time-integrated spectra presented in Fig. 11 were therefore computed as the sum of seven representative frames acquired prior to the onset of strong saturation in the Spec-KY video recording. Despite this, minor saturation effects persisted in three of the seven Spec-KY frames, specifically within the Mg I-2 and Na I-1 multiplets, as well as in the strongest Fe I-15 line at 526.95 nm. Normalisation of the Spec-KY profile to unity at the Fe I-15 peak at 526.95 nm consequently caused an artificial enhancement

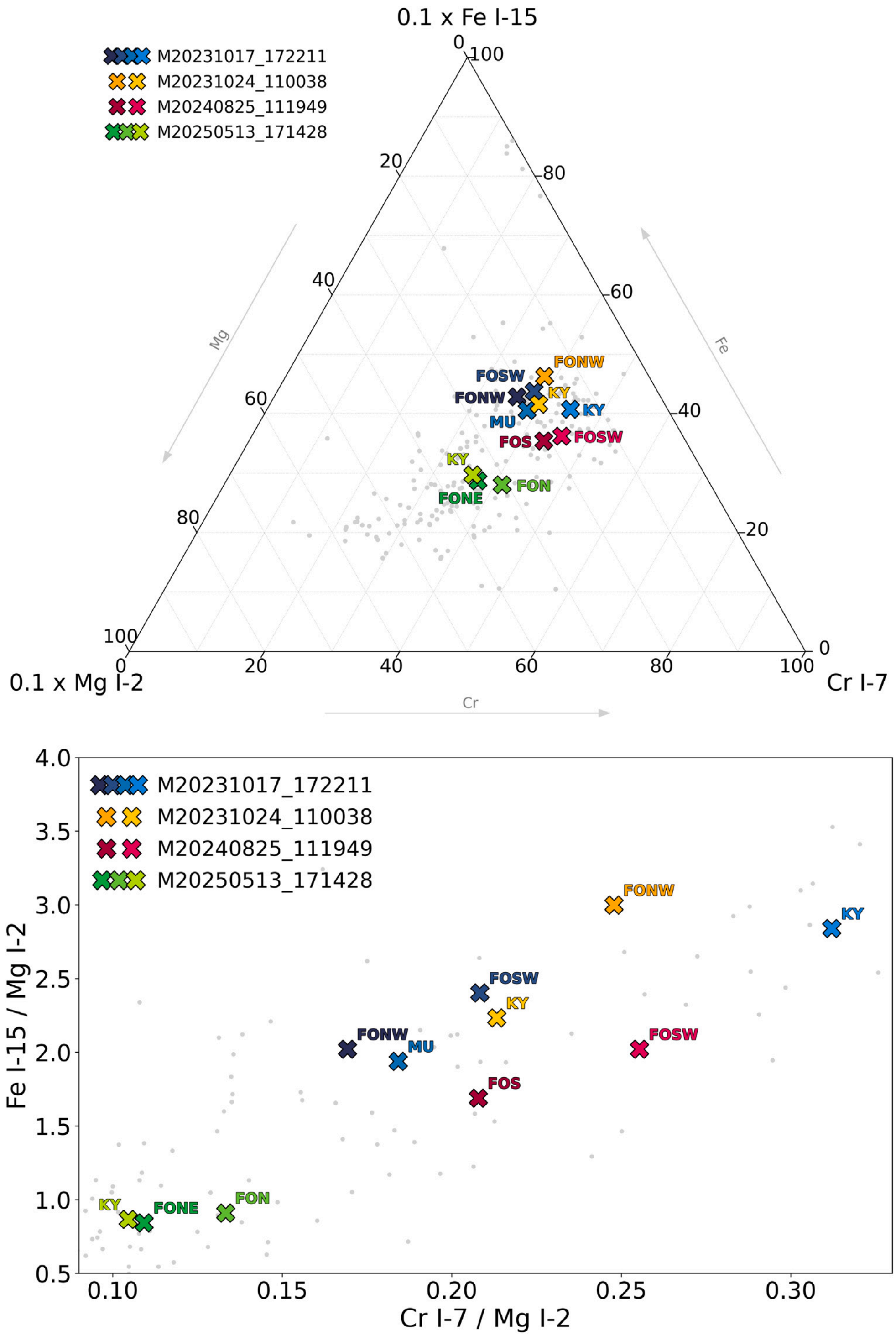

Fig. 8. Comparison of the relative intensities of multiplets Mg I-2, Cr I-7, and Fe I-15 derived from meteor spectra presented in this study. Upper panel: ternary diagram displaying the relative intensities of these multiplets across all spectral profiles. For clarity, the stronger Mg I-2 and Fe I-15 intensities have been scaled by a factor of 0.1 relative to the weaker Cr I-7. Lower panel: correlation between Fe I-15 and Cr I-7 intensities relative to the intensity of Mg I-2.

of the signal intensity across the spectral profile. To mitigate this effect, the M20231024_110038 spectra shown in Fig. 11 were normalised to unity at the Fe I-15 peak at 537.10 nm.

Despite the markedly different observing geometries of the Spec-KY and Spec-FONW spectrographs, the corresponding spectral profiles exhibit only a few significant discrepancies, as shown in Fig. 11. The majority of variations in spectral line intensities lie within the margin of error, as determined by the signal-to-noise (S/N) ratio, and can largely be attributed to the slightly reduced spectral resolution of the Spec-FONW spectrum relative to the Spec-KY profile. Representative examples of this effect include the Mn I-2 and Fe I-43 multiplets at approximately 403.30 nm and 404.58 nm, respectively, the Mg I-2 near 517.20 nm, and the Cr I-7 at approximately 520.60 nm. Furthermore, spectral lines in the near-UV region may be influenced by the reduced

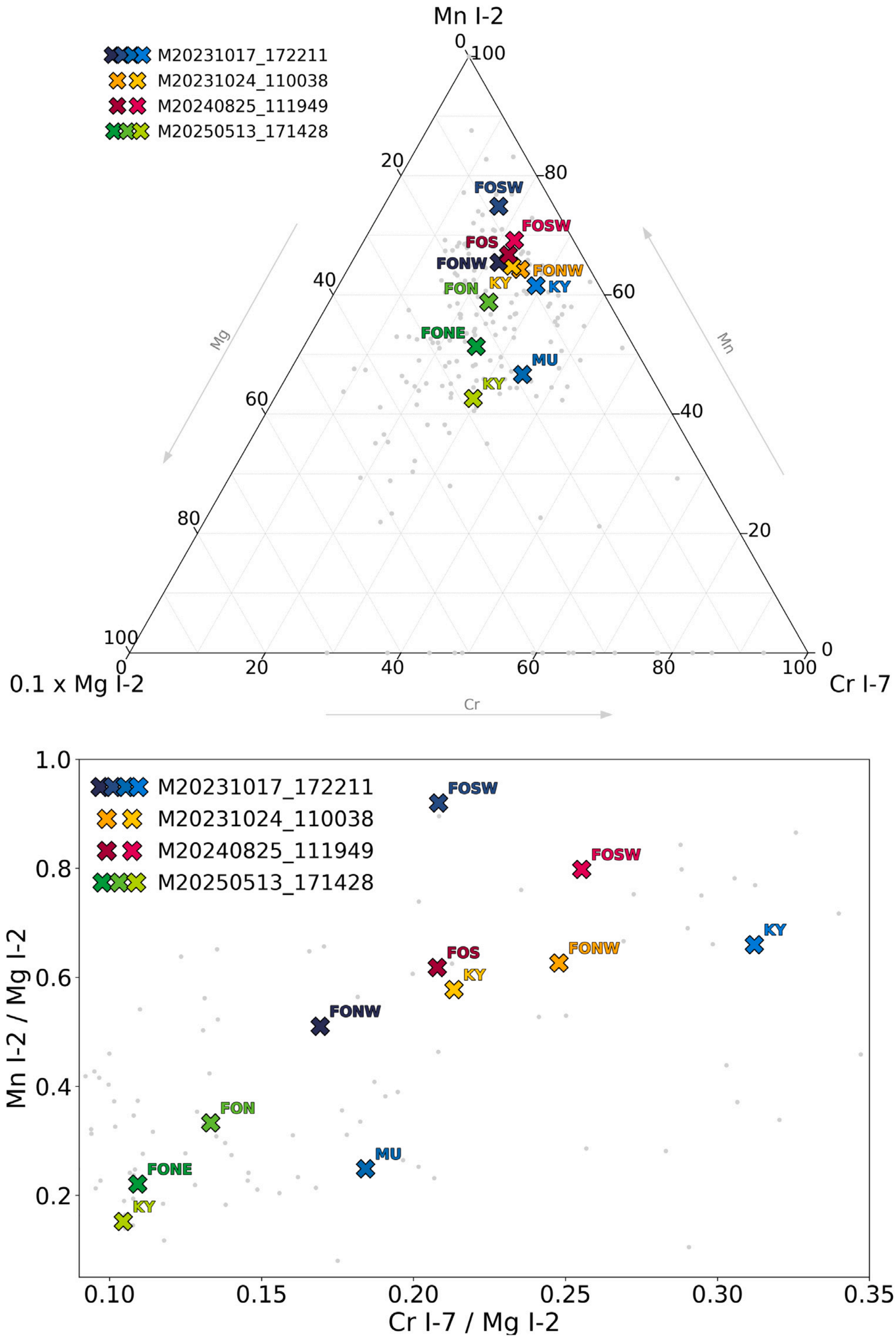

Fig. 9. Relative intensities of multiplets Mn I-2, Cr I-7, and Fe I-15 calculated for meteor spectra analysed in this work. Upper panel: ternary diagram displaying the relative intensities of these multiplets for all presented spectral profiles. The intensities of multiplet Fe I-15 were scaled by a factor of 0.1 to improve clarity of the plot. Lower panel: correlation between Mn I-2 and Cr I-7 intensities relative to the intensity of Mg I-2. In comparison with Fig. 7 and Fig. 8, the inclusion of Mn I-2 from the near-UV region produces a more pronounced dispersion in the case of meteors M20231017_172212 and M20250513_174828.

instrumental sensitivity as well as by uncertainties introduced through atmospheric extinction correction, as discussed in Section 3.1.

Although the Spec-KY time-integrated spectrum is affected by saturation more severely than the Spec-FONW profile, Fig. 11 reveals a pronounced enhancement in the Na I-1 intensity within the Spec-FONW spectrum. This effect is most likely attributable to differences in observing geometry. A near head-on orientation of Spec-KY may emphasise emission from the ablation front associated with the meteor head (Borovička, 1994; Kubelík et al., 2022), whereas the more oblique perspective of Spec-FONW could capture a greater contribution from the wake or trail emission, where low-excitation features such as Na I-1 are expected to be enhanced. Further discrepancies between the two profiles are evident in several Fe I lines across the spectrum. While the intensity variations of the Fe I-15 peak at 526.95 nm are most likely caused by saturation, differences observed in other, generally weaker Fe I lines can be attributed to the varying resolution of the

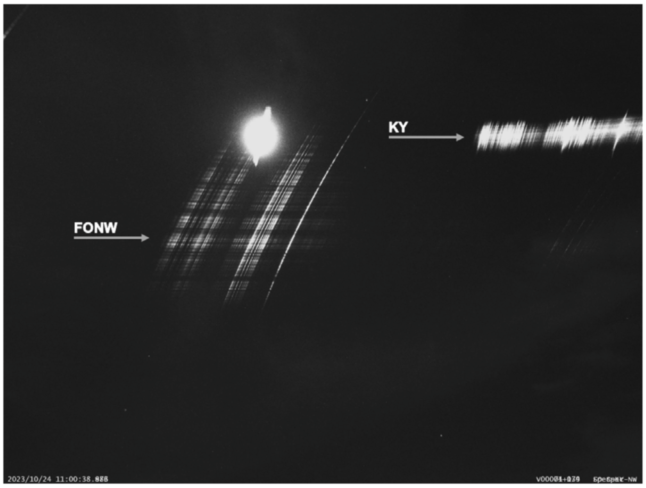

Fig. 10. Composite image of the spectrum of meteor M20231024_110038 observed by the AMOS spectrographs Spec-KY and Spec-FONW (Fig. 3).

Spec-FONW and Spec-KY profiles. Therefore, even though many of the Fe I peaks do not visually align between the Spec-KY and Spec-FONW spectra, their relative intensities are broadly comparable across both profiles. The discrepancy in Mn I-2 intensity reported in Section 3.1 is not observed in the M20231024_110038 profiles, likely because they represent only the initial phases of meteoroid ablation. During the early stages of ablation, the Mn I-2 signal in AMOS spectral data is typically weak but progressively increases over time, reflecting a gradual release. Beyond the gradual trend, sharp variations are sometimes observed during fragmentation events or flares, when localised pockets enriched in Mn and other refractory elements are ablated (Matlovič et al., 2026).

3.3. M20240825_111949

M20240825_111949 was a sporadic meteor with a typical asteroidal orbit, an initial speed of $v_i = 19.6\,\mathrm{km\,s^{-1}}$, and a maximum absolute magnitude of −7.6. Its spectrum was recorded by two AMOS spectrographs at Forrest — Spec-FOS and Spec-FOSW (Fig. 3), with both spectra covering similar portions of the spectrographs' FOVs (Fig. 12). As in the cases described in Sections 3.1 and 3.2, the spectrum of M20240825_111949 is broadly consistent with the profile expected for meteors originating from meteoroids of chondritic composition. Both captured profiles are characterised by strong Mg I, Fe I, and Na I emission, enhanced Mn I and Cr I features, and weak Ti I and Ni I emission (Fig. 13) and were calculated as sums of 20 representative frames extracted from the middle part of the meteor trajectory. Saturation affects the Na I-1 feature in both observed profiles, with a relatively minor influence also evident in the Mg I-2 multiplet recorded by Spec-FOSW. Saturation is presumably the major effect causing the variations of Na I-1 intensities extracted from the M20240825_111949 profiles (Figs. 7 and 13).

To account for the intensity variations observed in other lines present in the spectral profiles of M20240825_111949, a detailed examination indicates two major effects influencing them. First, the lines located below circa 390 nm are most likely affected by the applied calibrations, as they fall in the near-UV region where the AMOS-Spec-HR detector quantum efficiency and atmospheric transmission both decline steeply, so even small errors in the response function (Fig. 1) or applied extinction model (discussed in Section 3.1) can produce evident intensity deviations. Consequently, while the applied corrections improve the overall reliability of the spectra, they may also lead to variations displayed in the region below approximately 390 nm in Fig. 13.

The second effect is prevalent throughout the entire range of both M20240825_111949 profiles and arises from the differing spectral resolution of the Spec-FOS and Spec-FOSW observations. The average FWHM of lines in the Spec-FOS profile is 1.1 nm, whereas the average FWHM of Spec-FOSW lines is 1.4 nm, with several near-UV features exhibiting FWHM values up to 1.6 nm. The reduced resolving power of Spec-FOS at that time was most likely due to an unidentified hardware malfunction, which has since been corrected. As a result, effects such as line blending, the broadening of the line spread function leading to flux redistribution between line cores and wings, and the overall increase in the S/N ratio in lower-resolution spectra, enhanced the differences between the relative line intensities extracted from Spec-FOS and Spec-FOSW profiles, as demonstrated in Figs. 7 to 9. The multiplet most significantly affected by the spectral resolution differences is Fe I-15 (Fig. 7), which is consistently stronger in the higher-resolution Spec-FOSW profile relative intensities (Figs. 7 and 8). A similar effect is also evident for Spec-FOSW Cr I-7 and Mn I-2, albeit with smaller variations than in the case of Fe I-15 (Figs. 8 and 9). The variations observed in Mg I-2 are more likely attributable to saturation effects than to differences in resolving power.

The M20240825_111949 case is also suitable for demonstrating the relevance of the effects described by Šegon et al. (2024) for AMOS instrumentation, specifically the dependence of spectral response on the position within the field of view and the wavelength-dependent behaviour of the flat-field correction. To date, none of the AMOS meteor spectra observed simultaneously from multiple locations have proven to be strongly influenced by these effects. In all cases, other factors exerted a more significant impact on the observed spectra, as shown for the meteors discussed in Sections 3.1 and 3.2. Although the M20240825_111949 spectra positions significantly overlap in the Spec-FOS and Spec-FOSW FOVs, there is no indication that the observed variations in relative line intensities are visibly affected by the effects described in Šegon et al. (2024). To estimate their significance for the AMOS-Spec-HR setup, laboratory testing was conducted in which an AMOS-Spec-HR instrument was used to record spectra of a halogen–deuterium light source. The setup was tested for varying FOV positions of the source (zero order) and the first-order spectra. Comparing the normalised spectral intensity observed across different pixel ranges, i.e., different regions of the AMOS-Spec-HR camera detector plane, revealed strong consistency in the recorded signal regardless of FOV position. Coupled with the nearly linear diffraction efficiency of the AMOS-Spec-HR setup, this indicates that the instrument response is largely stable across the detector and does not introduce significant variations in the observed signal based on its FOV position or wavelength. Consequently, laboratory tests of the AMOS instrumentation indicated that the diffraction geometry described by Šegon et al. (2024) has only a minor effect on the relative line intensities extracted from AMOS spectral data. It should be noted, however, that these tests were conducted on a single AMOS-Spec-HR spectrograph setup. While minor variations among the AMOS spectrographs deployed worldwide cannot be excluded, such differences are not expected to be large enough to introduce significant biases into relative line intensities extracted from AMOS spectral data.

3.4. M20250513_171428

Meteor M20250513_171428 was identified to be a member of Epsilon Scorpiids (EPS, #660) meteor shower, first reported by Jenniskens et al. (2016). It was the fastest meteor among the four cases discussed in this work, with an initial speed of $v_i = 40.3\,\mathrm{km\,s^{-1}}$ and a maximum absolute magnitude of −9.1. Its spectrum was recorded by the Spec-FON, Spec-FONE, and Spec-KY instruments (Fig. 3), which captured high-quality spectra with an average FWHM of about 1.2 nm and almost no saturation (Fig. 14). The individual spectral profiles of M20250513_171428 shown in Fig. 15 are dominated by the Ca II-1 multiplet at 393.37 and 396.85 nm, Ca I-2 at 422.63 nm, Mg I-2,

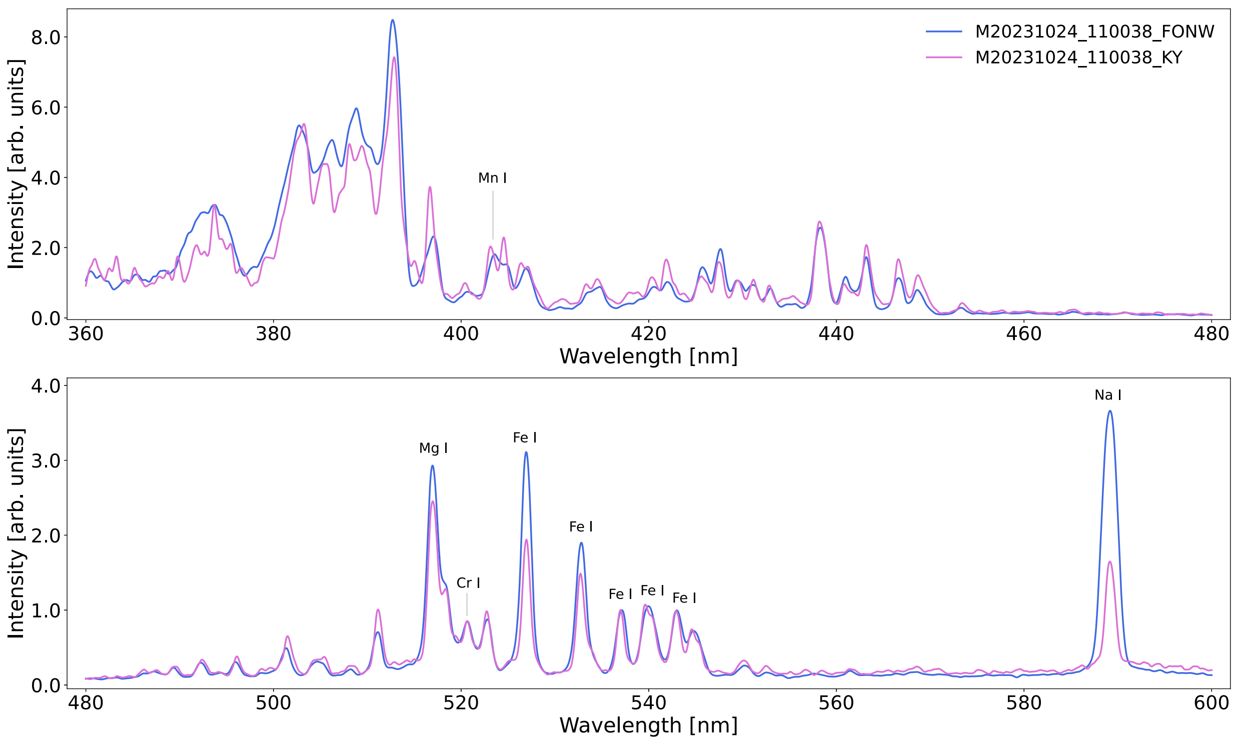

Fig. 11. Spectrum of meteor M20231024_110038 recorded by Spec-FONW and Spec-KY spectrographs (Fig. 3). The profiles are divided into two parts: 330–480 nm (upper panel) and 480–600 nm (lower panel), and are normalised to unity at the peak of Fe I-15 line at 537.10 nm to avoid the artificial increase of the Spec-KY signal caused by saturation of Fe I-15 strongest peak at 526.95 nm.

Fig. 12. Composite image of the recorded spectra of meteor M20240825_111949. The spectra occupy very similar positions in the FOVs of Spec-FOS and Spec-FOSW, resulting in their overlap within the image.

Na I-1, and several strong Fe I lines. Other notable features include Mn I-2 multiplet, Mg II-4 at 448.13 nm, and weaker Cr I-1 and Cr I-7 lines. The profiles also exhibit weak Ti I and Ni I emission. With almost no saturation present, the individual profiles were calculated as sums of all observed frames, meaning that the final time-integrated spectra encompass all phases of meteoroid ablation from beginning to end.

Fig. 15 demonstrates close correspondence across all three observed M20250513_171428 spectra, with more pronounced variations in the near-UV region, a feature typical of meteors observed simultaneously from multiple locations, as shown in previous sections. These differences are likely related to the applied calibration, particularly for the Spec-KY profile, which was recorded at low elevation (zenith angles of approximately 77–84°). In this case, the near-UV signal was strongly adjusted by atmospheric extinction calibration, and the attenuation below about 420 nm likely reflects absorption effects that were underestimated. Slight variations in spectral resolution between the individual observations may also contribute to discrepancies, as the Spec-FON profile, although of high quality, exhibited on average a larger FWHM than the other two by circa 0.2 nm. These effects are evident in the intensity of the Mn I-2 multiplet, as displayed in Fig. 9. Beyond the near-UV, however, all M20250513_171428 profiles show strong consistency, with differences most likely attributable to minor variations in FWHM, as illustrated by the Cr I-7 multiplet, which appears enhanced in the lower-quality Spec-FON profile (Fig. 8). Nevertheless, when comparing relative intensities of multiplets located in the wavelength range where detector sensitivity is highest (Fig. 1) and atmospheric extinction is weakest — between approximately 550 and 600 nm for the AMOS-Spec-HR — the relative line intensities yield a very precise match, as demonstrated for the Mg I-2, Fe I-15, and Na I-1 multiplets in Fig. 7.

The results of the M20250513_171428 analysis further support the weak influence of the effects studied by Šegon et al. (2024) on AMOS-Spec-HR spectra, as discussed in Section 3.3. Although the Spec-KY spectrum lies near the edge of the spectrograph's FOV and occupies a different portion of the FOV than Spec-FON and Spec-FONE, all spectra show close agreement in the measured relative line intensities. The minor differences identified in the profiles can be attributed to stronger factors mentioned in the previous paragraph. The influence of observing geometry in case of M20250513_171428 is most probably minimal. While the meteor was recorded by spectrographs installed at two separate locations, the relatively large distances between the meteor and the instruments (approximately 170 km for AMOS-FO and 300 km for AMOS-KY), combined with their relative positions and the nearly vertical atmospheric trajectory of M20250513_171428, ensured

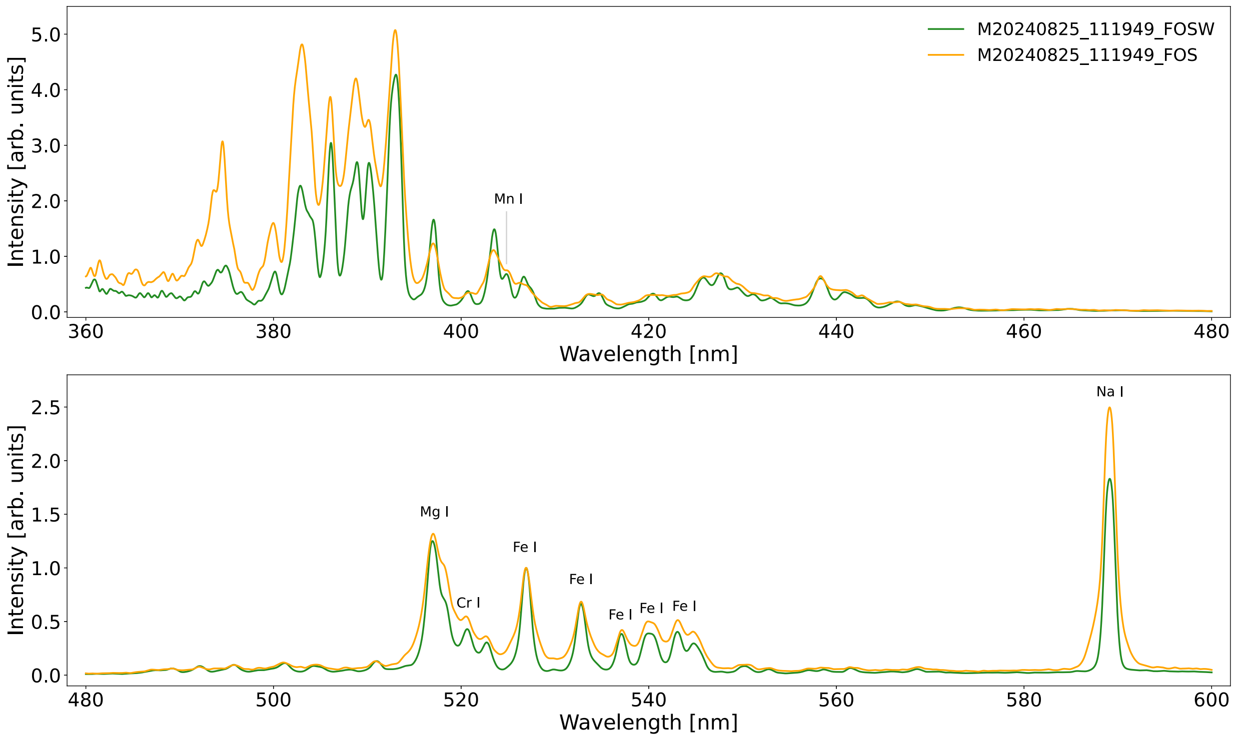

Fig. 13. Spectral profiles of meteor M20240825_111949 extracted from Spec-FOS and Spec-FOSW instruments (Fig. 3). The profiles are divided into two sections: 360–480 nm (upper panel) and 480–600 nm (lower panel). Both profiles are normalised to unity at the peak of Fe I-15 line at 526.95 nm. The Spec-FOS profile exhibits a notable reduction in spectral resolution compared to the Spec-FOSW profile.

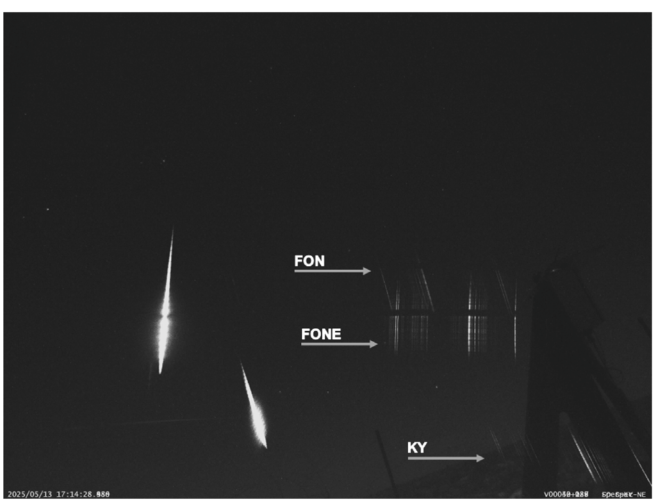

Fig. 14. Composite image of the M20250513_171428 meteor spectrum recorded by the Spec-FON, Spec-FONE, and Spec-KY spectrographs. The gap visible near the middle of the Spec-FONE zero-order image and its first-order spectrum is caused by a dropped video frame.

that all instruments most likely probed a very similar portion of the meteor plasma (Fig. 16). This is in accordance with the analysed profiles, which reveal only small variations among them.

4. Discussion

Although limited to just four events, the meteors described in this work provide a representative sample, as together they encompass a majority of the effects causing the relative line intensity variations in AMOS spectra recorded simultaneously from multiple locations. As demonstrated in Section 3, the primary sources of variation in multi-station spectral observations include:

- **Focusing.**
  AMOS-Spec-HR multi-station observations occasionally display variability in data quality, ranging from sharply focused spectra to those affected by imperfect focusing. Such issues may result from hardware malfunctions or environmental influences. Under ideal conditions, integrated line intensities derived from Gaussian profile fitting should remain stable, provided the detector response is fully linear and no flux is lost through excessive line broadening. In practice, however, several instrumental and processing effects can modify the measured values. For weak signals, the broadened wings of defocused lines may merge with background noise, truncating the Gaussian fit and leading to underestimation of the true flux. Background extraction may also not fully compensate for local background intensity variations once the zero-order meteor signal appears in the FOV, especially in case of very bright fireballs. Moreover, the choice of extraction aperture (the width of the scanning line used to isolate the spectrum) and the Gaussian fitting window can affect accuracy — inappropriate settings may yield either over- or underestimates of the actual line flux. These influences can be systematically assessed through laboratory simulations with controlled light sources. The impact of focusing in AMOS spectra has been evaluated as low to moderate, as shown in analyses of meteors M20231017_172212 (Section 3.1) and M20240825_111949 (Section 3.3), where focusing was identified as one of the primary factors contributing to discrepancies in relative line intensities extracted from the spectral profiles (Figs. 7 to 9).
- **Spectrum recording geometry.**
  Spectra recorded by systems installed at different locations are subject to variations in diffraction geometry. When a spectrum is observed at an acute angle relative to the grating orientation, partial signal overlap and line broadening can occur during spectrum

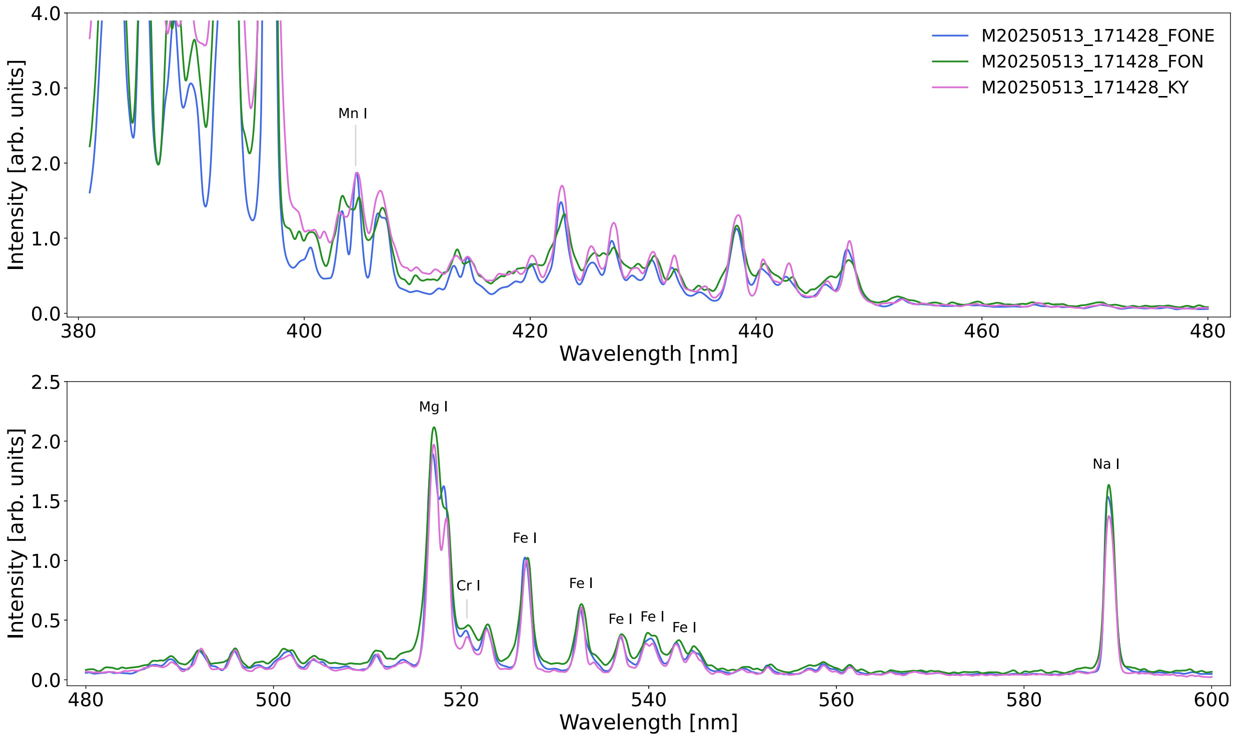

Fig. 15. Spectrum of meteor M20250513_171428 extracted from observations captured by Spec-FON, Spec-FONE, and Spec-KY spectrographs (Fig. 3). For clarity, the profiles are divided into two sections: 380–480 nm (upper panel) and 480–600 nm (lower panel). All three profiles are normalised to unity at the peak of Fe I-15 line at 526.95 nm.

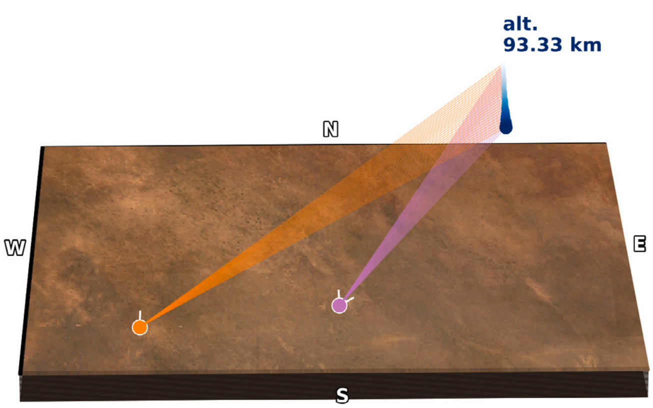

Fig. 16. Three-dimensional representation of the atmospheric trajectory of meteor M20250513_171428 (blue gradient) with respect to the AMOS instruments at Kybo and Forrest. The colours are consistent with the scheme applied in Fig. 3. White lines extending from each station mark the orientations of the Spec-KY, Spec-FON, and Spec-FONE spectrographs that captured the spectrum of M20250513_171428 with almost vertical atmospheric trajectory. The highlighted altitude corresponds to the beginning point of the meteor trajectory. (For interpretation of the references to colour in this figure legend, the reader is referred to the web version of this article.)

scanning and extraction. These effects arise from the projection of dispersed light onto the detector and may introduce distortions in the measured line profiles. While careful extraction using a narrow scanning aperture can mitigate the impact of this effect, further corrective options are limited. The influence of this effect is similar to the line broadening caused by focusing issues, but its overall impact is generally considered minor compared to other sources of variation in relative line intensities. The issues arising from the extraction geometry have been illustrated in the Spec-FONW profile of meteor M20231017_172212 (Section 3.1).

- **Observing and light path geometry.**
  Differences in the lines of sight between observing stations can introduce several physical effects that complicate the interpretation of spectral observations. First, the path length through the meteor plasma may vary between multiple systems, leading to differences in optical depth, self-absorption, and line-of-sight integration effects for specific species. These processes can alter relative line intensities depending on the amount of plasma traversed, but their magnitude is difficult to constrain without detailed radiative transfer modelling. Second, variations in viewing angle relative to the meteor trajectory may cause different portions of the shock front or ablation zone to be sampled. Since these regions can differ in temperature, density, and composition, the resulting spectra may emphasise different emission features, as demonstrated in modelling performed by Kubelík et al. (2022). This effect may be further amplified especially in cometary meteoroids, whose compositionally heterogeneous aggregate structure and fragmentation into fine-grained, compositionally diverse dust during ablation (eg. Rietmeijer 2008, Paquette et al. 2016, Vida et al. 2024) can introduce small-scale compositional inhomogeneities within the plasma column. Third, although not yet well understood in this context, meteor emission can be weakly polarised, and differences in optical path or viewing angle might cause slight variations depending on the instrument optics, a possibility that would benefit from verification in a dedicated future experiment. Finally, although Doppler shifts are theoretically expected to influence meteor spectra, they are negligible at the AMOS-Spec-HR resolution of $0.5\,\mathrm{nm\,px^{-1}}$. Even a head-on meteor with initial speed of $v_i \approx 72\,\mathrm{km\,s^{-1}}$, that should essentially yield the maximum Doppler shift possible for meteor spectra, would produce a shift of only 0.12 nm at 500 nm, and thus remains below AMOS-Spec-HR resolving power.

The influence of observing geometry in AMOS spectra has most likely been detected in the case of meteor M20231024_110038 (Section 3.2), where the head-on orientation of the meteor with respect to the Spec-KY instrument appears to have caused a marked decrease in the low-excitation Na I-1 doublet intensity compared to the profile obtained under a more oblique geometry. Tentative signs of this effect were also observed in the Mn I-2 intensity in the Spec-KY profile of meteor M20231017_172212 (Section 3.1). In summary, while the effects of observing and light-path geometry are physically plausible, reported in the literature (Kubelík et al., 2022), and can be explored through radiative transfer modelling, they remain difficult to characterise solely from observational data.

- **Atmospheric extinction correction.**
  Although the TAPAS service (Bertaux et al., 2014; Lallement et al., 2025) provides a reliable framework for atmospheric extinction correction, it is a model whose accuracy can vary with local atmospheric conditions such as aerosol content, humidity, and transient weather phenomena. Since models often rely on climatological averages and global datasets, they may not fully capture short-term or site-specific variations. In multi-station meteor observations, differences in zenith angle (altitude) relative to each observing station can introduce small but cumulative discrepancies in extinction correction. These differences affect the optical path length through the atmosphere, potentially leading to variations in the attenuation of certain spectral lines across stations. While such errors are generally minor, they can become significant in cases where spectra are compared quantitatively across multiple sites. It is important to note that this issue is especially pronounced for the Australian AMOS systems, where low site elevations and sparse local atmospheric data may make the TAPAS model inherently less reliable than at better-characterised mid-latitude sites.
  The impact of atmospheric extinction correction is most pronounced in the near-UV portion of meteor spectra, where extinction is strongest, and this effect is compounded by the lower sensitivity of the AMOS-Spec-HR detector in the near-UV. The combined consequence of these two factors has most likely been observed in all spectra discussed in Section 3. A robust estimation of the magnitude of this effect would require local meteorological measurements (e.g., aerosol optical depth, humidity profiles, or sky transparency) at each observing station, which is not feasible for the AMOS network. Overall, this influence is expected to be prominent particularly for meteors observed at large zenith angles, but is generally assumed to be weak, especially outside the near-UV.
- **Flat field and sensitivity drift.**
  Flat-field corrections are commonly used to compensate for variations in detector sensitivity and optical throughput across the FOV. In practice, however, they are inherently imperfect: their accuracy can degrade over time due to changes in instrument settings, detector aging, or gradual deterioration of optical components. Moreover, the optical elements themselves may introduce wavelength-dependent artefacts that are not fully accounted for in a single flat-field calibration. As a result, small imperfections in the flat fields can affect certain wavelengths more strongly than others, leading to subtle biases in the measured line intensities. Addressing this issue is challenging in routine meteor observations. Ideally, frequent and accurate sensitivity measurements would be performed, with each instrument recalibrated to track changes in detector response and optical throughput. In practice, this is difficult because AMOS instruments are installed worldwide, often in very remote areas. Flat-field images for the AMOS-Spec-HR are, therefore, acquired for each individual spectrograph before deployment to the observing location, under laboratory conditions using a uniformly illuminated white surface, and during the major camera servicing. An effective approach to addressing this issue is to characterise the wavelength and incidence-angle dependence of the flat field using a controlled laboratory setup as demonstrated by Šegon et al. (2024). The required level of detail in such calibration also depends on the optical configuration and the diffraction grating used, since many gratings exhibit a strong incidence-angle dependence of their diffraction efficiency. This effect can be particularly important for wide-FOV instruments: in this regard, AMOS systems with their smaller FOV compared to the all-sky cameras used by Šegon et al. (2024) are expected to be less affected, which is consistent with what has been observed in AMOS spectral data. Laboratory characterisation performed for the AMOS-Spec-HR instrument (Section 3.3) supports this expectation, indicating that these effects most likely have only a minor impact on AMOS spectral data. Nevertheless, more detailed testing would be necessary to precisely quantify the scale of these effects on AMOS spectra and to provide corrective measures if required. However, under typical observing conditions of the AMOS instruments, this effect is assumed to be minor, based on multi-station spectral observations analysed to date, including meteors M20240825_111949 (Section 3.3) and M20250513_171428 (Section 3.4).
- **Spectrograph throughput differences.**
  Partially related to the previous effect and to focusing, even when identical spectrograph setups are deployed at multiple stations, small differences in throughput are unavoidable. Manufacturing tolerances can lead to slight variations in grating efficiency or detector quantum efficiency, and these differences may become more pronounced over time as optical components age or degrade. As a result, the overall sensitivity of each system can diverge subtly, producing minor discrepancies in recorded line intensities across the AMOS network.
  In principle, throughput differences could be corrected by calibrating against standard stars with well-characterised spectra. However, this approach is difficult to implement in practice, since meteor spectrographs are not typically designed for stellar spectroscopy and may lack the necessary spectral coverage or calibration routines. An alternative, as noted previously, would be to perform accurate sensitivity measurements and calibrations on each system on a regular basis. This would allow wavelength-dependent throughput variations to be quantified and corrected, but the logistical demands of such frequent calibrations make this impractical for routine operations. Although almost certainly present to some extent in all spectra discussed in Section 3, these effects are assumed to be weak compared to other sources of variation considered in this work.
- **User input during processing and fitting.**
  AMOS spectral profiles are typically extracted and fitted manually (Section 2), which can introduce a degree of subjectivity into the analysis. Variations in the choice of extraction aperture width, background subtraction method, or the FWHM of fitted lines may accumulate, leading to minor differences in the evaluated relative line intensities depending on the specific approach adopted by the analyst. However, the tests conducted to assess the magnitude of this effect on AMOS spectral data indicate that such differences are generally very small and have only a minor impact on the overall accuracy of line intensity measurements.

A concise overview of these effects is provided in Table 1.

One of the central questions in the investigation of multi-station spectral observations is whether the above-mentioned effects influence the final relative line intensities to an extent that complicates the estimation of meteoroid composition. Figs. 7 to 9 show the relative line intensities of the Mn I-2, Mg I-2, Cr I-7, Fe I-15, and Na I-1 multiplets for all spectra of the four meteors analysed in this work. These multiplets were selected because they are frequently observed in meteor spectra and are particularly useful for meteoroid composition studies, as highlighted in works based on the spectral classification framework developed by Borovička et al. (2005) (e.g., Vojáček et al. (2015, 2019), Matlovič et al. (2019, 2020)) and more recently refined in Matlovič et al. (2024). The relative line intensities of all meteors with multiple spectral observations are compared against the remaining high-resolution AMOS spectral catalogue, which currently comprises 190 meteor spectra. This provides a broader context for the

Table 1
Overview of the effects influencing AMOS meteor spectra discussed in this work, including their estimated magnitude and potential approaches to mitigating their impact.

Cause	Possible effects	Magnitude	Correction measures
Focusing	Broadens and distorts spectral lines, causing flux loss, noise contamination, and biased fitting that leads to systematic intensity errors	Low to moderate	Laboratory tests with controlled sources and variable focus settings
Recording geometry	Introduces projection-related broadening and line overlap, distorting extracted profiles and biasing relative intensities	Variable (incident angle dependent)	Largely unresolvable due to random meteor incidence angles
Observing geometry	Changes the sampled plasma column depth and composition along the line of sight, affecting optical depth, self-absorption, and relative line contributions	Variable (geometry dependent)	Modelling spectra for different observing geometries
Atmospheric extinction correction	Biases line intensities in the near-UV due to uncertainties in extinction models and site-dependent atmospheric conditions	Variable (wavelength dependent)	Improving or reconsidering new extinction models, selecting optimal observing sites
Flat field and sensitivity drift	Introduces wavelength-dependent biases from temporal changes in detector response and optical throughput	Low	Controlled laboratory experiments, regular flat-field updates
Spectrograph throughput differences	Causes wavelength-dependent discrepancies in measured intensities between stations	Low	Calibration using standard stars, regular sensitivity monitoring
User input during processing	Introduces unpredictable, user-dependent biases during manual spectrum processing	Low	Transition to automated processing pipelines

dispersion of these ratios within a diverse dataset that includes chondritic and iron meteoroids, along with a small number of achondrite candidates (Matlovič et al., 2026).

As discussed in Section 3, all four meteors described in this work most likely originated from meteoroids with chondritic composition, based on the meteorite-based methodology of composition estimation proposed by Matlovič et al. (2024). The spectra of nearly all of these meteors share certain characteristics, such as overall similarity in the emission lines present in their profiles (Figs. 5, 11, 13 and 15) and Fe I emission enhancement (most clearly visible in Fig. 7) and their relative line intensities are generally consistent. A notable exception is meteor M20250513_171428, in which Fe I emission enhancement was not observed and the Na I-1 emission appeared diminished compared to the other three meteors (Fig. 7). This is likely attributable both to the higher entry speed of M20250513_171428 relative to the others — which attenuates the Na I-1/Mg I-2 intensity ratio compared to meteors with lower entry speeds (Borovička et al., 2005; Matlovič et al., 2019) — and to the fact that none of its profiles were affected by saturation.

In some cases, however, the differences between relative line intensities extracted from multiple profiles of the same meteor exceed those observed between different meteors. This is well illustrated in Fig. 7 for meteor M20231024_110038, whose Spec-KY profile yields relative line intensities that differ substantially from those of the Spec-FONW profile of the same meteor, and to a lesser extent for meteor M20240825_111949 in its Fe I-15 emission. A similar effect can be seen in Fig. 9 for the Mn I-2 emission of meteors M20231017_172212 and M20250513_171428. Although the differences in Mn I-2 intensities are relatively significant for this meteor (Section 3.4), it is important to note that, in general, more consistent results for Mn I-2 would be achieved if it were expressed in relative ratios with adjacent lines rather than with more distant ones such as Mg I-2 or Cr I-7. This approach ensures that all compared lines are affected by similar calibration-related errors, thereby minimising the influence of these effects on meteoroid composition estimation.

As discussed in Section 3, a majority of the variations in relative line intensities extracted from multi-station spectral observations of meteors can be explained by the effects described above. Some of these influences are more pronounced in specific wavelength ranges, such as non-ideal calibrations in the near-UV, while most can affect the entire observed spectrum. The origin of certain variations, however, cannot be clarified until they are observed in a larger sample of multi-station spectral data. One example is the behaviour of Cr I emission in the profiles of meteor M20231024_110038. While the intensity of the Cr I-1 multiplet lines is notably weaker in the head-on Spec-KY spectrum, the Cr I-7 lines appear unaffected (Fig. 11). To date, this phenomenon has been observed only in the case of M20231024_110038 and requires further study to determine whether it represents a real physical effect or a random fluctuation.

The case of M20250513_171428 demonstrates that if the multi-station spectral observation is largely unaffected by the sources mentioned in this section, the relative line intensities obtained from the respective spectra exhibit a very good agreement (Figs. 5, 11, 13 and 15). By contrast, if the specific spectra are affected by them, they can exhibit more or less significant variations. In all meteors presented in this work, that represent a larger sample of AMOS multi-station spectral observations analysed so far, these variations have generally been of low to moderate magnitude for the instrumentation used and most of the more significant variations between the profiles and resulting relative line intensities could be attributed to specific effects. It is therefore unlikely that these effects would hinder meteoroid composition estimation, provided they are properly considered in the interpretation of meteor spectra.

5. Conclusions

This work presents one of the few analyses of meteor spectra observed simultaneously from multiple observing sites. Using four meteors as representative examples of a larger set of multi-station spectral observations obtained by the AMOS network, we demonstrated the variations between spectra of the same meteor captured from multiple observing stations. The most significant effects influencing the multi-station meteor spectra identified are focusing, spectrum extraction geometry, observing and light-path geometry, and imperfect flat-field and atmospheric extinction calibrations. Less pronounced influences include throughput differences between AMOS-Spec-HR spectrographs and user-dependent variability introduced by the manual spectral processing approach. While these effects are largely specific to the AMOS-Spec-HR instrumentation, they are expected to occur in other systems, albeit to different extents. We observed that when the spectra of a given meteor are largely unaffected by these phenomena, the relative line intensities extracted from all observations show very good correspondence. In contrast, when these effects are present, they can induce variations of differing magnitude. The strongest discrepancies in multi-station spectral observations were associated with focusing issues, which tended to over- or underestimate the intensities of nearly all spectral features, observing geometry, as illustrated by a meteor recorded head-on with respect to the AMOS-Spec-HR instrument that exhibited a significant decrease in Na I-1 intensity compared to a more oblique viewpoint, and calibration errors, particularly imperfect atmospheric extinction corrections, which predominantly affect features in the near-UV.

Despite these variations, we conclude that careful consideration of these effects during spectral processing ensures that the precision of meteoroid composition estimation based on the relative line intensities is not compromised. Furthermore, the insights gained from multi-station spectral observations can be applied to single-station spectra, where the effects identified in this study can be recognised and accounted for. This approach has the potential to further improve the accuracy of meteoroid composition estimates based on relative line intensities extracted from significantly more frequent single-station observations of meteor spectra.

CRediT authorship contribution statement

Veronika Pazderová: Writing – review & editing, Writing – original draft, Visualization, Formal analysis, Conceptualization. **Pavol Matlovič:** Writing – review & editing, Funding acquisition, Formal analysis, Conceptualization. **Hadrien A.R. Devillepoix:** Investigation, Data curation.

Declaration of competing interest

The authors declare that they have no known competing financial interests or personal relationships that could have appeared to influence the work reported in this paper.

Acknowledgements

This work was supported by European Space Agency (ESA) under contract no. 4000140012/22/NL/SC/rp, by the Slovak Grant Agency for Science grant VEGA 1/0218/22, and by the Slovak Research and Development Agency, Slovak Republic grants VV-MVP-24-0232 and APVV-23-0323.

References

Abe, S., 2009. Meteoroids and meteors - observations and connection to parent bodies. In: Lecture Notes in Physics, vol. 758, pp. 1–38. http://dx.doi.org/10.1007/978-3-540-76935-4_5.

Bertaux, J.L., Lallement, R., Ferron, S., Boonne, C., Bodichon, R., 2014. TAPAS: A web-based service of atmospheric transmission computation for astronomy. Astron. Astrophys. 564, A46. http://dx.doi.org/10.1051/0004-6361/201322383, arXiv:1311.4169.

Borovička, J., 1993. A fireball spectrum analysis. Astron. Astrophys. 279 (2), 627–645, URL: https://ui.adsabs.harvard.edu/abs/1993A&A...279..627B.

Borovička, J., 1994. Two components in meteor spectra. Planet. Space Sci. 42 (2), 145–150. http://dx.doi.org/10.1016/0032-0633(94)90025-6, URL: https://www.sciencedirect.com/science/article/pii/0032063394900256. Special issue: Asteroids, Comets and Meteors 1993-I.

Borovička, J., Koten, P., Spurný, P., Boček, J., Štork, R., 2005. A survey of meteor spectra and orbits: evidence for three populations of Na-free meteoroids. Icarus 174 (1), 15–30. http://dx.doi.org/10.1016/j.icarus.2004.09.011, URL: https://www.sciencedirect.com/science/article/pii/S001910350400301X.

Devillepoix, H.A.R., Tóth, J., Matlovič, P., Cupák, M., Towner, M.C., Sansom, E.K., Kornoš, L., Paulech, T., Zigo, P., 2022. A meteor spectroscopic survey in the nullarbor. Res. Notes AAS 6 (7), 144. http://dx.doi.org/10.3847/2515-5172/ac81ce.

Drouard, A., Vernazza, P., Loehle, S., Gattacceca, J., Vaubaillon, J., Zanda, B., Birlan, M., Bouley, S., Colas, F., Eberhart, M., Hermann, T., Jorda, L., Marmo, C., Meindl, A., Oefele, R., Zamkotsian, F., Zander, F., 2018. Probing the use of spectroscopy to determine the meteoritic analogues of meteors. Astron. Astrophys. 613, A54. http://dx.doi.org/10.1051/0004-6361/201732225, URL: https://ui.adsabs.harvard.edu/abs/2018A&A...613A..54D. arXiv:1802.04699.

Ferus, M., Koukal, J., Lenža, L., Srba, J., Kubelík, P., Laitl, V., Zanozina, E.M., Váňa, P., Kaiserová, T., Knížek, A., Rimmer, P., Chatzitheodoridis, E., Civiš, S., 2018. Calibration-free quantitative elemental analysis of meteor plasma using reference laser-induced breakdown spectroscopy of meteorite samples. Astron. Astrophys. 610, A73. http://dx.doi.org/10.1051/0004-6361/201629950, URL: https://ui.adsabs.harvard.edu/abs/2018A&A...610A..73F.

Jenniskens, P., 2007. Quantitative meteor spectroscopy: Elemental abundances. Adv. Space Res. 39 (4), 491–512. http://dx.doi.org/10.1016/j.asr.2007.03.040, URL: https://www.sciencedirect.com/science/article/pii/S0273117707002633.

Jenniskens, P., Nénon, Q., Gural, P.S., Albers, J., Haberman, B., Johnson, B., Morales, R., Grigsby, B.J., Samuels, D., Johannink, C., 2016. CAMS newly detected meteor showers and the sporadic background. Icarus 266, 384–409. http://dx.doi.org/10.1016/j.icarus.2015.11.009, URL: https://www.sciencedirect.com/science/article/pii/S0019103515005199.

Kasuga, T., Yamamoto, T., Watanabe, J., Ebizuka, N., Kawakita, H., Yano, H., 2005. Metallic abundances of the 2002 leonid meteor deduced from high-definition TV spectra. Astron. Astrophys. 435 (1), 341–351. http://dx.doi.org/10.1051/0004-6361:20041428.

Kornoš, L., Ďuriš, F., Tóth, J., 2018. AMOS orbit software, EDMOND database. In: Gyssens, M., Rault, J.-L. (Eds.), Proceedings of the International Meteor Conference, Petnica, Serbia, 2017. p. 46.

Kubelík, P., Koukal, J., Lenža, L., Srba, J., Laitl, V., Křížová, R., Křivková, A., Civiš, S., Chernov, V.E., Ferus, M., 2022. Probing plasma physics and elemental composition of a leonid meteor by fitting complex plasma radiation model parameters. Mon. Not. R. Astron. Soc. 514 (4), 5266–5275. http://dx.doi.org/10.1093/mnras/stac1600.

Lallement, R., Bertaux, J.L., Ferron, S., Boonne, C., Richard, E., Lefèvre, F., Smoker, J.V., 2025. Transmission of the atmosphere for astronomical data: TAPAS upgrade. Astron. Astrophys. 701, A200. http://dx.doi.org/10.1051/0004-6361/202555022.

Matlovič, P., Pisarčíková, A., Pazderová, V., Loehle, S., Tóth, J., Ferrière, L., Čermák, P., Leiser, D., Vaubaillon, J., Ravichandran, R., 2024. Spectral properties of ablating meteorite samples for improved meteoroid composition diagnostics. Astron. Astrophys. 689, A323. http://dx.doi.org/10.1051/0004-6361/202450913.

Matlovič, P., Pisarčíková, A., Pazderová, V., Vörös, T., Hlobik, F., Devillepoix, H.A.R., Borovička, J., Paprskárová, M., Deam, S.E., Tóth, J., Kornoš, L., Paulech, T., Zigo, P., 2026. Achondrites in meteor data: Spectra, dynamics, and physical properties of candidate aubrite and eucrite impactors. Astron. Astrophys. 706, A247. http://dx.doi.org/10.1051/0004-6361/202558248.

Matlovič, P., Tóth, J., Kornoš, L., Loehle, S., 2020. On the sodium enhancement in spectra of slow meteors and the origin of Na-rich meteoroids. Icarus 347, 113817. http://dx.doi.org/10.1016/j.icarus.2020.113817, URL: https://www.sciencedirect.com/science/article/pii/S0019103520301986.

Matlovič, P., Tóth, J., Rudawska, R., Kornoš, L., Pisarčíková, A., 2019. Spectral and orbital survey of medium-sized meteoroids. Astron. Astrophys. 629, A71. http://dx.doi.org/10.1051/0004-6361/201936093.

Moore, C.E., 1945. A multiplet table of astrophysical interest. Revised edition. Part I - Table of multiplets. 20, pp. 1–110, Contributions from the Princeton University Observatory.

Paquette, J.A., Engrand, C., Stenzel, O., Hilchenbach, M., Kissel, J., 2016. Searching for calcium–aluminum-rich inclusions in cometary particles with Rosetta/COSIMA. Meteorit. Planet. Sci. 51 (7), 1340–1352. http://dx.doi.org/10.1111/maps.12669.

Rietmeijer, F.J.M., 2008. Natural variations in comet-aggregate meteoroid compositions. Earth Moon Planets 102 (1–4), 461–471. http://dx.doi.org/10.1007/s11038-007-9164-4.

Šegon, M., Borovička, J., 2023. Transition to digital meteor spectra: A study in progress. In: Pajer, U., Kereszturi, A., Steyaert, C., Rendtel, J., Rudawska, R., Verbeeck, C., Gyssens, M., Ocana, F. (Eds.), Proceedings of the International Meteor Conference 2022. pp. 70–73, URL: https://ui.adsabs.harvard.edu/abs/2023pimo.conf...70S.

Šegon, M., Vojáček, V., Borovička, J., 2024. Improvements in digital meteor spectra reduction. Exp. Astron. 57, http://dx.doi.org/10.1007/s10686-024-09933-z.

Spurný, P., Borovička, J., Shrbený, L., Hankey, M., Neubert, R., 2024. Atmospheric entry and fragmentation of the small asteroid 2024 BX1: Bolide trajectory, orbit, dynamics, light curve, and spectrum. Astron. Astrophys. 686, A67. http://dx.doi.org/10.1051/0004-6361/202449735.

Tóth, J., Kornoš, L., Duriš, F., Matlovič, P., Zigo, P., Kalmančok, D., Paulech, T., Šimon, J., Baláž, M., Vörös, T., Paprskárová, M., Pazderová, V., Solčáni, J., Schichman, M., Varga, P., 2026. AMOS global meteor network: Instrumentation, procedures, accuracy validation and results. Icarus 454, 117086. http://dx.doi.org/10.1016/j.icarus.2026.117086.

Tóth, J., Matlovič, P., Loehle, S., Vaubaillon, J., Pisarčíková, A., Leiser, D., Grigat, F., Eberhart, M., Hufgard, F., Ravichandran, R., Poloni, E., Hoerner, I., Duernhofer, C., Delahaie, S., Ferrière, L., Rommeluere, S., Rambaux, N., 2024. Overview of the MetSpec project: Artificial meteors in ground testing. Icarus 407, 115791. http://dx.doi.org/10.1016/j.icarus.2023.115791, URL: https://www.sciencedirect.com/science/article/pii/S001910352300369X.

Trigo-Rodríguez, J.M., Llorca, J., Borovička, J., Fabregat, J., 2003. Chemical abundances determined from meteor spectra: I. Ratios of the main chemical elements. Meteorit. Planet. Sci. http://dx.doi.org/10.1111/j.1945-5100.2003.tb00313.x, URL: http://hdl.handle.net/10150/655740.

Vida, D., Brown, P.G., Campbell-Brown, M., Egal, A., 2024. First holistic modelling of meteoroid ablation and fragmentation: A case study of the orionids recorded by the Canadian automated meteor observatory. Icarus 408, 115842. http://dx.doi.org/10.1016/j.icarus.2023.115842, URL: https://www.sciencedirect.com/science/article/pii/S0019103523004219.

Vojáček, V., Borovička, J., Koten, P., Spurný, P., Štork, R., 2015. Catalogue of representative meteor spectra. Astron. Astrophys. 580, A67. http://dx.doi.org/10.1051/0004-6361/201425047.

Vojáček, V., Borovička, J., Koten, P., Spurný, P., Štork, R., 2019. Properties of small meteoroids studied by meteor video observations. Astron. Astrophys. 621, A68. http://dx.doi.org/10.1051/0004-6361/201833289.

Wojdyr, M., 2010. Fityk: A general-purpose peak fitting program. J. Appl. Crystallogr. 43, 1126–1128. http://dx.doi.org/10.1107/S0021889810030499.

von Zahn, U., Gerding, M., Höffner, J., McNeil, W.J., Murad, E., 1999. Iron, calcium, and potassium atom densities in the trails of Leonids and other meteors: Strong evidence for differential ablation. Meteorit. Planet. Sci. 34 (6), 1017–1027. http://dx.doi.org/10.1111/j.1945-5100.1999.tb01419.x.